Analysis of zero-frequency solutions of the pion dispersion equation in nuclear matter

V. A. Sadovnikova

Petersburg Nuclear Physics Institute,
Gatchina, St. Petersburg 188300, Russia

Abstract

In this paper we consider instability of nuclear matter which takes place when the frequencies of the collective excitations turn to zero. We investigate collective excitations with pion quantum numbers $J^\pi = 0^-$. We study the dependence of zero-frequency solutions of the pion dispersion equation on the value of the spin-isospin quasiparticle interaction G'. The solutions of the pion dispersion equation describe the different types of the excitations in the matter, $\omega_i(k)$. At the critical density $\rho = \rho_c$ one of solutions of the definite type turns to zero: $\omega_{i0}(k_c){=}0$. When $\rho > \rho_c$, the excitations $\omega_{i0}(k)$ become amplified. It is shown that there is such a "transitional" value of $G' = G'_{tr}$ that for $G' < G'_{tr}$ the zero-frequency solutions belong to the type ω_{sd} while for $G' > G'_{tr}$ they pertain to the type ω_c. The solutions of the type ω_{sd} correspond to instability to small density fluctuations of the nuclear matter at $G' \leq -1$. On the other hand, ω_c is responsible for the "pion condensation" at $G' \approx 2$. For the stable nuclear matter the branches of solutions $\omega_{sd}(k)$ and $\omega_c(k)$ are located on the unphysical sheets of the complex plane of frequency.

1   Introduction

In this paper we investigate the excitations of nuclear matter with the pion quantum numbers. Our analysis is based on studies the in-medium pion dispersion equation. Interactions of pions with baryons in nuclear matter is included in framework of Migdal model [1]. Solutions of the pion dispersion equation in this model were considered on the physical sheet of the complex plane of pion frequency ω. We expand this analysis to the unphysical sheets of the Riemann surfaces. We have included first the unphysical sheets to the analysis in our earlier papers [2, 3]. In [2, 3] we studied the branches of solutions responsible for the pion condensation and the long wavelength instability and it was shown that they are the separate branches supplemented to the well-known zero-sound, pion, and isobar ones.

In this paper we continue to study the solutions of zero-sound and pion dispersion equations responsible for the instability of nuclear matter using the retarded pion propagator. We analyze zero-frequency solutions of the pion dispersion equation depending on the value of G' and define to what type excitations these zero-frequency solutions refer. This could permit us to do conclusion about the character of the phase transition related to the considered instability.

Except the purely theoretical interest the problem has various applications. Investigation of the pion excitations in nuclear matter, started long ago, continue to play an important role in nuclear physics. Special interest in study of the pionic many-body degrees of freedom was stimulated by prediction and investigation of the pion condensation [1, 4, 5, 6]. In recent years the study of the pionic many-body degrees of freedom is related to the investigations of the excited states and of phase transitions in nuclear matter in heavy ion collisions. Detailed knowledge of in-medium pion dynamics is essentially important for description of mesons ([1, 6]), nucleons ([2]) and Δ-isobars [7], [8]. Analysis of the dilepton production from $\pi^+ - \pi^-$ annihilation requires the knowledge of the pion dispersion in hot and dense matter [8, 9, 10].

To study of the pion dynamics in heavy ion collisions we need the relativistic description of the pion self-energy at the finite temperatures. Solutions of the relativistic pion dispersion equations were presented in papers [11, 12]. A pion self-energy with the correct nonrelativistic limit was obtained in papers [13, 14].

When considering the pion dynamics in nuclear matter at high densities and temperatures, it is important to have as a "point of reference" a reliable description of the nuclear matter excitations with pion quantum numbers in nonrelativistic limit. Such description have been obtained in the pioneering papers of Migdal and his group [1], followed by the numerous papers [5, 6, 15, 16, 17, 18].

In this paper we study the solutions of the nonrelativistic pion dispersion equations in symmetric nuclear matter at zero temperature following to [1]. The aim of this paper is to study the solutions with zero frequency ω=0 depending on the value of the coupling constant G'. These solutions characterize the stability boundary (in this model it is the boundary on the density). In this paper it is shown that at different values of G' the zero-frequency solutions belong to the different types of excitations.

The value of G' is considered in the interval $-1 \leq G' \leq 2$. When we change G', the branches of solutions are changed as well: certain solutions go over from the physical to unphysical sheets and vice verse. To identify the solutions on the unphysical sheets it is important to know the solutions on the physical ones. The branches of solutions which are obtained in the present paper reproduce the results of [1, 19, 20] on the physical sheet of the complex plane of ω. To do comparison with other papers the simple model with the constant effective quasiparticle interaction is very useful. However, the pion condensation in this model emerges at too low density and this is not consistent with the results of investigations, [1].

It is well known that the solutions of the pion dispersion equations, $\omega_i(k)$, describe the different types of excitations in the nuclear matter. They are: spin-isospin zero-sound wave, $\omega_s(k)$, pion wave, $\omega_\pi(k)$, isobar wave, $\omega_\Delta(k)$, and others [1, 5, 6, 21]. The appearance of the solution with ω=0 means that at the certain values of nuclear density $\rho = \rho_c$ and wave vector $k = k_c$ the frequency of a definite type of excitations i_0 turns to zero: $\omega_{i_0}(k_c)$=0. If $\rho > \rho_c$ one obtains $Im\omega_{i_0}(k) > 0$, and the amplified solution takes place. This signals the instability of nuclear matter. The change of G' causes the changes of the values of ρ_c and k_c. Moreover, at a special situation zero-frequency solution passes to another type of excitations i_1: $\omega_{i_1}(k_c)$=0. It was shown in [22] that the phase transition is determined by the type of those excitations which become unstable. Thus it is important to know to what type of excitations the solutions with ω=0 belongs.

In Fig. 1 we show the values of critical densities ρ_c and wave vectors k_c for which the

pion dispersion equation

$$D^{-1} = \omega^2 - k^2 - m_\pi^2 - \Pi^R(\omega, k) = 0 \ , \tag{1}$$

has solutions with $\omega=0$ at any value of G'. We are interested in solutions which satisfy additional restriction: $\left(\frac{d}{dk}\omega(k)\right)_{k=k_c}=0$. In Eq. (1) $\Pi^R(\omega, k)$ is the pion self-energy part (retarded polarization operator). The pion self-energy is formed on the basic of particle-hole and isobar-hole loops renormalized due to the effective interactions of quasiparticles: G'_{NN}, $G'_{N\Delta}$ and $G'_{\Delta\Delta}$. (The effective constant G' is regarded as G'_{NN} through the paper.) In Fig. 1 the critical density ρ_c and wave vector k_c are presented for three models of the pion self-energy. The matter is stable at $\rho < \rho_c$ for the every model. The physical variables which are related to the pion propagator D diverge along the curves in Fig. 1. This corresponds to the phase transition [22] in nuclear matter. At $\rho < \rho_c$, the nuclear matter is considered as a normal Fermi liquid, but at $\rho > \rho_c$ there is phase transitions into new state which may include the standing spin-isospin wave or "condensates of excitation".

Let us introduce the useful definitions. The waves $\omega_s(k)$, $\omega_\pi(k)$, $\omega_\Delta(k)$, and others we name branches of solutions. The set of branches of solutions of the same type for the different values of G' composes a family (ω_s, ω_π, ω_Δ, and others). When we say about zero-frequency solutions or $\omega=0$ solutions, we mean that the condition $\left(\frac{d}{dk}\omega(k)\right)_{k=k_c}=0$ is satisfied in this point, as well.

Return to Fig. 1. There are known two reasons for instability in the framework of Migdal theory [1] in the nonrelativistic symmetric cold nuclear matter at not too high densities. In paper [23] it was shown that Fermi liquid becomes unstable when the attractions between the quasiparticles is too strong. In spin-isospin channel this corresponds to $G' < -1$ [1]. In Fig. 1 we see that there are not solutions with $\omega=0$ at $G' < -1$. This is because of the matter is unstable at the any density. Another region of $G' \approx 2$ corresponds to the instability in respect to transition into a new ground state containing condensate of pions [1]. In the present paper the main attention is paid to study that families of solutions which are responsible for instability along the curves in Fig. 1, from long wavelength instability to pion condensation.

We start with the analysis of the zero-sound dispersion equation for spin-isospin excitations with quantum numbers $J^\pi = 0^-$. This equation is closely related to the pion dispersion equation. It was shown in paper [22, 24] that for the case of strong attraction between the quasiparticles ($G' < -1$) the zero-sound dispersion equation has a growing with time solution which corresponds to instability in response of small-amplitude, long wavelength density fluctuations. For $G' > -1$ the unstable solutions do not appear [19, 20].

In this paper the family of solutions responsible for the long wavelength instability is built. We denote this family as ω_{sd}. The index "sd" means "spinodal decomposition". It is known [22], that the thermodynamic stability condition requires the partial derivative of the pressure with respect to the volume to be negative, i.e., $\left(\frac{\partial P}{\partial V}\right)_T < 0$. The process which takes place in matter, when this condition is broken, is known as a spinodal decomposition [25]. It is shown in [22], that there is a relation between the effective quasiparticle interaction and the partial derivative

$$\frac{\partial P}{\partial V} = -\frac{N}{V^2} \frac{p_F^2}{3m}(1 + F_0),$$

N is the number of particles, F_0 is the effective scalar-isoscalar quasiparticle interaction. The stability condition is broken at $F_0 < -1$. For the zero-sound dispersion equation this

corresponds to the appearance of the imaginary amplified solutions. It looks reasonable to use the notation $\omega_{sd}(k)$ for such solutions. Here we use the same notation for the analogous solutions, which appear in the spin-isospin channel at $G' < -1$. Moreover, as it is shown below, at $G' < 0$ all the solutions belong to the same family. We use the notation $\omega_{sd}(k)$ for them as well. The branches $\omega_{sd}(k)$ are imaginary and can be found for all values $G' < 0$.

Now we turn to the pion dispersion equation. In the channel of excitations with the pion quantum numbers the particle-hole interaction can be modified by taking into account the pion-nucleon interactions [1]. As a result, collective and particle-hole excitations are renormalized due to interaction with pions and, vice versa, the pion excitations are changed due to interaction with particle-hole ones in the nuclear matter. It was predicted [1, 4], that the account of the pion-nucleon interaction is responsible for the phase transition into the ground state with the pion condensation. In Fig. 1 it is demonstrated that due to the pion-nucleon interaction we obtain the phase transition not only for $G' < -1$ but for all (considered) values of G'.

For the pion dispersion equation (1) we can find the branch of solutions corresponding to $\omega_{sd}(k)$. We denote it as $\omega_{sd}^{\pi}(k)$. The correspondence is established in the following way. It will be seen from the form of the pion self-energy that $\omega_{sd}(k)$ are the poles of $\Pi(\omega, k)$, and for each value of k the frequency $\omega_{sd}^{\pi}(k)$ tends to $\omega_{sd}(k)$ as pion-nucleon coupling constant $f_{\pi NN} \to 0$.

We show also that there is a special value of G', denoted by G_{tr} ($|G'_{tr}| \ll 1$). When $G' < G'_{tr}$, the solutions with $\omega{=}0$ are on the branches $\omega_{sd}^{\pi}(k)$. When $G' > G'_{tr}$, the type of the family carrying zero-frequency solutions is changed. We shall refer to G'_{tr} as "transition value".

When $G' > G'_{tr}$, zero-frequency solutions pass to the branches of solutions of another family. It is denoted as ω_c ("condensate"). The solutions of (1) referred to this family, $\omega_c(k)$, are identified in the following way. In papers [1] it was shown that among the solutions of the pion dispersion equation the imaginary solutions emerge under special conditions. Instability of matter, related to these imaginary solutions is interpreted as a phase transitions into a new ground state containing the pion condensate. The branch $\omega_c(k)$ reproduces the imaginary solutions presented in [1] on the physical sheet of ω. It is demonstrated that ω_c is an independent family of solutions along with ω_π, ω_s, ω_Δ or ω_{sd}^{π} and it is responsible for pion condensation.

In Sect. 2 the expressions for the retarded pion self-energy are presented and the singularities on the complex plane are investigated. We consider the structure of the Riemann surfaces that are defined by the form of the pion self-energy. The unphysical sheets are described.

In Sect. 3 the family ω_{sd} is considered for the zero-sound and pion dispersion equations. It is shown how zero-frequency solutions $\omega_{sd}(k_c){=}0$ at $\rho = \rho_c$ (Fig. 1) come these branches.

In Sect. 4 the different types of solutions of the pion dispersion equation are considered on the physical and unphysical sheets. It is shown that there is an independent family of solutions ω_c that is related to the pion condensation.

In Sect. 5 we determine the value of G'_{tr} and show how the solution with $\omega{=}0$ pass from the family $\omega_{sd}^{\pi}(k)$ to $\omega_c(k)$ when $G' = G'_{tr}$.

In this paper we solve the dispersion equations in the symmetric nuclear matter with

zero temperature. The equilibrium density is ρ_0, p_{F0}=0.268 GeV. During the computations, the effective mass of quasiparticles is assumed to be m=0.8m_0, while m_0=0.94 GeV is the vacuum nucleon mass. The pion mass is m_π=0.14 GeV, the isobar mass $\Delta = 1.23$ GeV (the isobar width is neglected). Following to the paper [1], the effective nucleon quasiparticle interaction can be written as

$$\mathcal{F}(\vec{k}_1, \vec{\sigma}_1, \vec{\tau}_1; \vec{k}_2, \vec{\sigma}_2, \vec{\tau}_2) = C_0(F(\vec{k}_1, \vec{k}_2) + F'(\vec{k}_1, \vec{k}_2)(\vec{\tau}_1\vec{\tau}_2) + G(\vec{k}_1, \vec{k}_2)(\vec{\sigma}_1\vec{\sigma}_2)$$

$$+G'(\vec{k}_1, \vec{k}_2)(\vec{\sigma}_1\vec{\sigma}_2)(\vec{\tau}_1\vec{\tau}_2)),$$

where $\vec{\tau}, \vec{\sigma}$ are the Pauli matrices in the isospin and spin spaces. The factor $C_0 = N_0^{-1}$, where N_0 is a density of states for two sorts of nucleon on the Fermi surfaces, $N_0 = 2p_F m/\pi^2$; F, F', G, G' are the Landau-Migdal dimensionless parameters. In this paper we use a simple model where parameters are taken to be a constant: $G'(\vec{k}_1, \vec{k}_2) = G'(p_F, p_F) \equiv G'$. The Landau-Migdal parameter G' found from the analysis of the nuclear experimental data is $G' \sim 1.5 - 1.7$ [15, 26]. This parameter describes the short-range correlations between the nucleons with a range $\sim \frac{1}{m_0}$: $V_{corr} = \frac{f^2}{m_\pi^2}g'(\vec{\sigma}_1\vec{\sigma}_2)(\vec{\tau}_1\vec{\tau}_2)$. The relation $G' = \frac{1}{C_0}\frac{f^2}{m_\pi^2}g'$ sets the correspondence of the Landau-Migdal parameters to the effective correlative parameters g' [11, 12, 13].

The Landau-Migdal parameter $G' = G'_{NN}$ corresponds to rescattering of $NN \leftrightarrow NN$ quasiparticles. The parameters $G'_{N\Delta}$ and $G'_{\Delta\Delta}$ determine the rescattering of $N\Delta \leftrightarrow NN$ and $N\Delta \leftrightarrow N\Delta$. The parameters $G'_{N\Delta}$ and $G'_{\Delta\Delta}$ are not changed in the course of paper and are taken equal to $G'_{N\Delta}$=0.4 and $G'_{\Delta\Delta}$=1.6 [1].

In the paper we take the pion-nucleon coupling constant $f_{\pi NN} = 1$ and the pion-nucleon-isobar coupling constant $f_{\pi N\Delta} = 2$.

2 The pion self-energy $\Pi(\omega, k)$

In this Section we present the expressions for the pion self-energy in nuclear matter. These expressions are well known [1, 21, 24, 27, 28]. We do an analytical continuation in ω of the polarization operator $\Pi(\omega, k)$ to the unphysical sheets of the complex plane. The search of zero-frequency solutions is related to investigation of the solutions both on the physical and unphysical sheets.

We consider excitations in nuclear matter which are described by the solutions of the pion dispersion equation (1). The causality requirement leads to the known interpretation of the solutions of the dispersion equation in the complex plane of ω. The stable excitations are described by the solutions with real frequencies, placed on the real axis. The damping solutions (resonances) are placed on the unphysical sheets under the cuts, which the polarization operator has on the real axis. This is Landau damping which is related to overlapping of the frequency of excitations with the frequency of free particle-hole pairs (which give the imaginary part in the pion self-energy). We can introduce the damping of solutions in another way, with the help of the isobar width (taken as the experimental constant, Γ=115 MeV) or quasiparticle damping constant, for example. In this case the real excitations are displaced to the lower half plane of the physical sheet [2, 3]. We do not consider this damping henceforth.

At certain conditions (large density, a strong attraction between particles) the imaginary solutions arise in the upper half-plane of the physical sheet. They correspond to the excitations with amplify amplitude. Such excitations correspond to an unstable regime. We find the corresponding solutions with negative imaginary part in the lower half-plane of the physical sheet, as well.

The amplified solutions in the spin-isospin channel (as well as all the solutions with $Re\omega_i > 0$) are interpreted, following [1, 29], as the frequencies of π^+-type excitations. While the solutions in the lower half-plane (as well as all the solutions with $Re\omega_i < 0$) are considered as π^--type excitations. Their frequencies have to be taken with an opposite sign in respect to the solutions. For the physical excitations of π^0-type we put into correspondence the solutions with $Re\omega_i > 0$. In symmetrical nuclear matter with $N = Z$ all three types of solutions, i.e., π^+, π^-, π^0 are identical. In the asymmetric nuclear matter the solutions carrying different charges are transformed in a different way with the change of the parameter of asymmetry and of the density. The method used in this paper permits to follow these transformations from symmetric up to neutron nuclear matter.

Pion self-energy in nuclear matter is due to S- and P-interaction of the pions and nucleons. The total pion self-energy is thus a sum of a scalar and vector terms:

$$\Pi(\omega, k) = \Pi_S(\omega, k) + \Pi_P(\omega, k) . \tag{2}$$

The main results of this paper are obtained for $\Pi(\omega, k) = \Pi_P(\omega, k)$ operator. One can consider some models for $\Pi_S(\omega, k)$ and they give the expressions like $\Pi_S = const \cdot \rho$ without ω and k dependence [2, 21]. The influence of Π_S on the final results has the quantitative character and is discussed in Appendix A.

2.1 P-wave part of the pion self-energy, $\Pi_P(\omega, k)$

Following the papers [1, 24, 27] we write $\Pi_P(\omega, k)$ as a sum of the nucleon and isobar parts

$$\Pi_P(\omega, k) = \Pi_N(\omega, k) + \Pi_\Delta(\omega, k) . \tag{3}$$

The operators $\Pi_N(\omega, k)$ and $\Pi_\Delta(\omega, k)$ can be expressed through the lowest order polarization insertions $\Pi_N^0(\omega, k)$ and $\Pi_\Delta^0(\omega, k)$ which can be presented as the integrals over the particle-hole (Φ_N) and isobar-hole loops (Φ_Δ). The vertices of these loops are described by the pion-nucleon and isobar-nucleon-pion coupling constants $f_{\pi NN}$, $f_{\pi N\Delta}$ and by the form factors which take the nonzero baryon size into account, $d_B(k^2) = \frac{\Lambda_B^2 - m_\pi^2}{\Lambda_B^2 + k^2}$, where $B = N, \Lambda$ and $\Lambda_N = 0.667$ GeV, $\Lambda_\Delta = 1.0$ GeV. Polarization operators $\Pi_N^0(\omega, k)$, $\Pi_\Delta^0(\omega, k)$ can be written as:

$$\Pi_N^0(\omega, k) = -4(\frac{f_{\pi NN}}{m_\pi})^2 k^2 d_N^2(k^2)\Phi_N(\omega, k), \tag{4}$$

$$\Pi_\Delta^0(\omega, k) = -\frac{16}{9}(\frac{f_{\pi N\Delta}}{m_\pi})^2 k^2 d_\Delta^2(k^2)\Phi_\Delta(\omega, k). \tag{5}$$

Then for Π_N, Π_Δ we have the expressions [28]:

$$\Pi_N(\omega, k) = \Pi_N^0(\omega, k)\frac{1 + C_0(\alpha(k)G'_{N\Delta} - G'_{\Delta\Delta})\frac{-16}{9}\Phi_\Delta(\omega, k)}{E(\omega, k)},$$

$$\Pi_\Delta(\omega, k) = \Pi_\Delta^0(\omega, k) \frac{1 + C_0(\frac{1}{\alpha(k)}G'_{N\Delta} - G'_{NN})(-4)\Phi_N(\omega, k)}{E(\omega, k)}. \tag{6}$$

In this equation $\alpha(k) = (\frac{4}{3}f_{\pi N\Delta}d_\Delta(k^2))/(2f_{\pi NN}d_N(k^2))$. In Eqs. (6) we see that $\Pi_N(\omega, k)$ is $\Pi_N^0(\omega, k)$ with one vertex renormalized due to nucleon-hole and isobar-hole interaction. The denominator $E(\omega, k)$ has a form

$$
\begin{aligned}
E(\omega, k) &= 1 + C_0 \left(4G'_{NN}\Phi_N(\omega, k) + \frac{16}{9}G'_{\Delta\Delta}\Phi_\Delta(\omega, k) \right. \\
&\quad \left. + 4\frac{16}{9}C_0(G'_{NN}G'_{\Delta\Delta} - G'^2_{N\Delta})\Phi_N(\omega, k)\Phi_\Delta(\omega, k) \right)
\end{aligned}
\tag{7}
$$

and the condition

$$E(\omega, k) = 0 \tag{8}$$

gives a zero-sound dispersion equation. Solutions of this equation describe the excitations in nuclear matter, if we do not take into account the renormalization due to the pion-baryon interaction. Equation (1) has the solutions corresponding to the solutions of Eq. (8). Thus at $G'_{NN} < 0$, Eq. (8) has the solutions $\omega_{sd}(k)$ (which will be shown and discussed below), while at $G'_{NN} > 0$ there are zero-sound solutions $\omega_s(k)$ [19, 20, 22]. These solutions are the poles of $\Pi_N(\omega, k)$ and $\Pi_\Delta(\omega, k)$ (6). The equation (1) has the corresponding solutions: $\omega_{sd}^\pi(k)$ and $\omega_s^\pi(k)$. It can be seen from the structure of Eq. (1) that when $f_{\pi NN}$ and $f_{\pi N\Delta}$ approach zero points, the branches $\omega_{sd}^\pi(k)$ ($\omega_s^\pi(k)$) approach to the poles of polarization operator $\Pi(\omega, k)$, i.e., $\omega_s(k)$ ($\omega_{sd}(k)$).

2.2 Extension of $\Pi_N^0(\omega, k)$ in ω to the unphysical sheets of the complex plane

The causal polarization operator $\Pi_N^0(\omega, k)$ can be presented as a sum of two terms, the first term corresponds to excitation and the second to the annihilation of the particle-hole pairs. We want to study the excitations in nuclear matter which appear as a response on an external perturbation and we use the retarded operators in Eq. (1). For the real ω they are determined as [22, 27]

$$\Pi^{0R}(\omega, k) = (Re + i\ sign(\omega)Im)\Pi^0(\omega, k)$$

and $\Phi_N^R(\omega, k)$ is expressed through the integrals [27]

$$\Phi_N^R(\omega, k) = \frac{-1}{(2\pi)^3} \int d^3p \left[\frac{\theta(|\vec{p} + \vec{k}| - p_F)\theta(p_F - p)}{\omega + \frac{p^2}{2m} - \frac{(\vec{p}+\vec{k})^2}{2m} + i\eta} - \frac{\theta(p - p_F)\theta(p_F - |\vec{p} + \vec{k}|)}{\omega + \frac{p^2}{2m} - \frac{(\vec{p}+\vec{k})^2}{2m} + i\eta} \right]. \tag{9}$$

The function $\Phi_N^R(\omega, k)$ can be written as

$$\Phi_N(\omega, k) = \phi_N(\omega, k) + \phi_N(-\omega, k). \tag{10}$$

The first integral in (9) corresponds to $\phi(\omega, k)$ and the second one to $\phi(-\omega, k)$. Equation (9) can be used to obtain a condition which relates the values of $\Phi_N^R(\omega, k)$ in the two points of the complex plane [22]

$$\Phi_N^R(-\omega^*, k) = \Phi_N^{R*}(\omega, k). \tag{11}$$

The same equation can be written for Φ_Δ^R and, consequently, for operators in Eqs. (3)-(7). Henceforth only the retarded operators are used and index R is omitted.

We write the expression for $\Phi_N(\omega, k)$ in such a way that it does not contain the overlapping logarithm cuts (compare with [24, 27]):

$$\phi_N(\omega, k) = \frac{m}{k} \frac{1}{4\pi^2} \left(\frac{-\omega m + k p_F}{2} - \omega m \ln \left(\frac{\omega m}{\omega m - k p_F + \frac{1}{2}k^2} \right) \right. \tag{12}$$

$$\left. + \frac{(k p_F)^2 - (\omega m - \frac{1}{2}k^2)^2}{2k^2} \ln \left(\frac{\omega m - k p_F - \frac{1}{2}k^2}{\omega m - k p_F + \frac{1}{2}k^2} \right) \right)$$

for $0 \leq k \leq 2p_F$. Each of logarithms has its own region of integration over p and over the angle between $\vec{p}$ and $\vec{k}$ in (9). These regions are shown in [27].

At $k \geq 2p_F$, $\phi_N(\omega, k)$ is the Migdal's function [1, 21]

$$\phi_N(\omega, k) = \frac{1}{4\pi^2} \frac{m^3}{k^3} \left[\frac{a^2 - b^2}{2} \ln \left(\frac{a+b}{a-b} \right) - ab \right] \tag{13}$$

where $a = \omega - (k^2/2m)$, $b = k p_F/m$.

Function $\Phi_\Delta(\omega, k) = \phi_\Delta(\omega, k) + \phi_\Delta(-\omega, k)$, where $\phi_\Delta(\omega, k)$ is determined by (13) with $a = \omega - (k^2/2m) + (m_\Delta - m)$.

Let us consider the cuts of $\Pi_N^0(\omega, k)$ in the complex plane of ω. It is clear that, for $k \leq 2p_F$, there are two cuts (we denote them by I and II). The cuts originated by the logarithmic terms of (12) are at

$$I : 0 \leq \omega \leq \frac{k p_F}{m} - \frac{k^2}{2m} \tag{14}$$

$$II : \frac{k p_F}{m} - \frac{k^2}{2m} \leq \omega \leq \frac{k p_F}{m} + \frac{k^2}{2m} \; .$$

The cuts of the function $\phi_N(-\omega, k)$ lie on the negative semi-axis symmetrically with respect to the cuts in (14). Therefore, $\Pi_N^0(\omega, k)$ has four cuts in the complex plane of ω, which are shown in Fig. 2. When $\omega > 0$, the cuts are caused by the singularities of $\phi_N(\omega, k)$, while at $\omega < 0$ the cuts are related to the logarithms of $\phi_N(-\omega, k)$.

The imaginary factors in denominators in (9) determine the physical sheet in the complex plane of frequency. On the physical sheet the first logarithm in (12) has the imaginary part on the upper edge of the cut I equal to $-\pi i$, and $+\pi i$ on the lower edge of the cut. In the point $\omega m - k p_F + \frac{1}{2}k^2 = 0$, where the cuts I and II touch each other, the imaginary part of $\phi_N(\omega, k)$ is continuous but there is a jump of the derivative. This is shown in [27], Fig. 12.9.

Let us now determine the unphysical sheets which we pass on when go under the cuts I and I' (Fig. 2). Consider the cut I. We denote the first logarithm in (12) as $ln(z_1) \equiv ln \left(\frac{\omega m}{\omega m - k p_F + \frac{1}{2}k^2} \right)$. While the frequency ω goes along the cut I (14): $\omega = (0, \frac{k p_F}{m} - \frac{k^2}{2m})$ then z_1 is changed in the interval $z_1 = (0, -\infty)$. The cut I in the complex plane of ω corresponds to the cut along the negative real axis in the complex plane of z_1. When we go to the cut I from above (the arrow in Fig. 2a), this corresponds that we go to the cut from below in the complex plane of z_1. Going over under the cut, we pass on to the unphysical sheet neighboring with the physical one on the Riemann surface of $ln(z_1)$. The values of $ln(z_1)$ on the neighboring

sheet differ by of $(-2\pi i)$ from the values on the physical one at the same ω. As example, the value of $ln\left(\frac{\omega m}{\omega m - kp_F + \frac{1}{2}k^2}\right)$ on the lower edge of cut I is $ln\left(-\frac{\omega m}{\omega m - kp_F + \frac{1}{2}k^2}\right) + \pi i$. But the value at the same point of ω on the unphysical sheet is $ln\left(-\frac{\omega m}{\omega m - kp_F + \frac{1}{2}k^2}\right) - \pi i$. Thus, we have the continuous changing of logarithm along the arrow in Fig. 2a. Then we conclude that $\Pi(\omega, k)$ in Eq. (1) changes continuously as well. Thus, going over under the cut I in Fig. 2a we pass on to the unphysical sheet of the complex plane of ω that is placed under the physical sheet. Let us denote the unphysical sheet with the same letter as a cut: I. The part of the unphysical sheet I is shown in Fig. 2b by the shading with the right slope.

Now we define an unphysical sheet related to the cut I' (denote the sheet by I'). The cut I' stems from the first logarithm in $\phi(-\omega, k)$. We designate $ln(z_1') \equiv -ln\left(\frac{-\omega m}{-\omega m - kp_F + \frac{1}{2}k^2}\right) = ln\left(\frac{\omega m + kp_F - \frac{1}{2}k^2}{\omega m}\right)$. Going over under the cut of $ln(z_1')$ we add the shift $-2\pi i$ to the value of $ln(z_1')$. Then, the logarithm on the sheet I' under the lower edge of the cut I' is equal to $ln\left(-\frac{\omega m + kp_F - \frac{1}{2}k^2}{\omega m}\right) + \pi i - 2\pi i$. This expression is used for the analytical continuation to the sheet I'. The part of the sheet I' is shown on the Fig. 2b by the shading with the left slope.

In the paper we consider the solutions of (1) which are placed on the shaded parts of the unphysical sheets I and I' in Fig. 2b. Each logarithmic term in (10), (12) has its own Riemann surface. An important point here is that moving on Riemann surface of one of logarithms we stand on the physical sheet for the other logarithms.

Thus, we have built up two unphysical sheets I and I'. Let us show that the values of $\Pi_N^0(\omega, k)$ are real and coincide on the negative imaginary axes of the sheets I and I'.

On the imaginary axis we denote $\omega = i\omega_i$. On the negative imaginary axis of the sheet I, the function Φ_N (10), (12) takes a form

$$\Phi_N(i\omega_i, k) = \frac{mp_F}{4\pi^2}\left[1 - \frac{i\omega_i m}{kp_F}\left(\ln\frac{-i\omega_i m}{i\omega_i m - kp_F + \frac{1}{2}k^2} - \pi i\right)\right. \tag{15}$$

$$\left. - \frac{i\omega_i m}{kp_F}\left(\ln\frac{i\omega_i m + kp_F - \frac{1}{2}k^2}{i\omega_i m}\right) + \dots\right].$$

$$= \frac{mp_F}{4\pi^2}\left[1 + 2\frac{\omega_i m}{kp_F}\left(arctg\frac{\omega_i m}{kp_F - \frac{1}{2}k^2} - \frac{\pi}{2}\right) + \dots\right]. \tag{16}$$

Here only the first and the second terms of $\phi(\omega, k)$ and $\phi(-\omega, k)$ (12) are shown.

On the other hand, on the negative imaginary axis of the sheets I' the function Φ_N (10) is

$$\Phi_N(i\omega_i, k) = \frac{mp_F}{4\pi^2}\left[1 - \frac{i\omega_i m}{kp_F}\ln\frac{i\omega_i m}{i\omega_i m - kp_F + \frac{1}{2}k^2}\right. \tag{17}$$

$$\left. - \frac{i\omega_i m}{kp_F}\left(\ln\frac{i\omega_i m + kp_F - \frac{1}{2}k^2}{-i\omega_i m} - \pi i\right) + \dots\right]$$

and after reduction we have the expression (16) again. This is the illustration of the following connection between the values of $\Pi_N^0(\omega, k)$ on I and I' sheets:

$$\left(\Pi_N^0(\omega, k)\right)_I^* = \left(\Pi_N^0(-\omega^*, k)\right)_{I'}. \tag{18}$$

Thus, $\Pi_N^0(\omega, k)$ is defined on the lower semiplanes of the unphysical sheets I and I' (the shaded regions in Fig. 2b), and the values of $\Pi_N^0(\omega, k)$ coincide on the negative imaginary axes of the sheets I and I'. The special solutions of (1) which we are interested in, are placed on the shaded part of the complex plane of ω in Fig. 2b and on the imaginary axes of the physical and unphysical sheets.

3   Investigation of instability at $G'_{NN} < G'_{tr}$

In this part we consider solutions of the pion dispersion equation (1) at $G'_{NN} < G'_{tr}$. The definition of G'_{tr} will be given in the Sect. 5, since it is determined by the behavior of branches which are studied in Sects. 3,4. We start by considering the zero-sound dispersion equation, and investigate its solutions for different values of G'_{NN}. We demonstrate the modification of these solutions when we pass to the pion dispersion equation.

3.1   Zero-sound dispersion equation

In this Subsection we consider the unstable solutions $\omega_{sd}(k)$ of the zero-sound dispersion equation. For $G'_{NN} < -1$, they are amplified, placed on the physical sheet and reflect the instability of nuclear matter in respect to the small fluctuations of density. For $-1 < G' < 0$, the branches $\omega_{sd}(k)$ are damped, and come to the negative imaginary axes (which belongs to the unphysical sheets I and I').

In this Section we do not take into account the excitations of isobar and restrict ourselves by $\Pi(\omega, k) = \Pi_P(\omega, k)$ in (3). The zero-sound dispersion equation stems from (8) and has the form

$$- 4C_0 \Phi_N(\omega, k) = \frac{1}{G'}. \tag{19}$$

The results obtained for this equation are valid both in spin-isospin and in isoscalar, spin, isoscalar channels.

First we obtain the solutions of Eq. (19) in the kinetic theory of Landau and compare them with the known results. The function $\Phi_N(\omega, k)$ (10,12) in the long wavelenths limit is

$$\Phi_N(\omega, k) = 2 \frac{m p_F}{4\pi^2} \left(1 - \frac{\omega m}{2 k p_F} \ln \frac{\frac{\omega m}{k p_F} + 1}{\frac{\omega m}{k p_F} - 1} \right). \tag{20}$$

Substituting this expression in (19), we obtain the known zero-sound dispersion equation [22]

$$1 + \frac{1}{G'} = \frac{\omega m}{2 k p_F} ln \left(\frac{\omega m + k p_F}{\omega m - k p_F} \right) = \frac{s}{2} \ln \frac{s+1}{s-1}. \tag{21}$$

Here we denote $s = \frac{\omega m}{k p_F}$. When $G' < -1$, this equation has two (positive and negative) solutions on the imaginary axis of the physical sheet [22, 24]. Let us denote $s = i\gamma$, then Eq. (21) transforms into

$$1 + \frac{1}{G'} = \gamma \, arctg \frac{1}{\gamma} . \tag{22}$$

To obtain solutions for $-1 < G' < 0$, we take the long wavelength limit of Eq. (16) and substitute it in (19). On the negative imaginary axis of the unphysical sheet, we get an

equation

$$1 + \frac{1}{G'} = -\gamma(arctg(\gamma) - \frac{\pi}{2}). \tag{23}$$

Solutions of this equation are negative, i.e., $\gamma < 0$. This equation coincides with that presented in paper [19]. It was pointed out in [19] that the solution of Eq. (23) " do not correspond to an actual solution". In agreement with this statement we see that solutions of (23) are located on the negative imaginary axis belonging both I and I' unphysical sheets. It was explained in [19] the damping of this mode is the Landau damping [22].

In Fig. 3 the solutions γ to Eq. (19) are shown at $G' < 0$. They are similar to the solutions at $G' < 0$ in Fig. 1 of [19] (except the curve ab at $-1 < G' < 0$). The shaded region means that the solution are on the unphysical sheets. In Fig. 3 it is demonstrated that when the attraction between the particles is increasing, the damping solution placed on the unphysical sheet goes over to the physical sheet, turning to amplified solution.

Considering the unphysical sheets we can find two solutions of (19) for any value of $G' < 0$ (Fig. 3). However, at $-1 < G' < 0$ they are on the different unphysical sheets. It was shown that the solutions of Eq. (23) are negative thus being located on the unphysical sheet I. Now we look for solutions with $\gamma > 0$ (curve ab in Fig. 3). The situation is the same as we had with the sheets I and I'. There are two new unphysical sheets $\tilde{I}$ and $\tilde{I}'$ which overlay the physical one. In Appendix B the construction of these sheets is presented. The dispersion equation (19) on the imaginary positive unphysical axis is the same on the both $\tilde{I}$ and $\tilde{I}'$ sheets and has a form

$$1 + \frac{1}{G'} = -\gamma(arctg(\gamma) + \frac{\pi}{2}). \tag{24}$$

The solutions of this equation are positive. This equation turns into Eq. (23) if to change the sign of γ. The solutions of this equation are shown by the curve ab in Fig. 3. They are located on the positive imaginary unphysical axis (this is marked by the horizontal shading).

Let us compare Fig. 3 and Fig. 1 in [20]. In paper [20] only one curve is presented which corresponds to decreasing of γ with increasing of G'. This curve describes the physical processes: the amplifying of the amplitudes of the small fluctuations at $G' < -1$ and the Landau damping of excitations at $-1 < G' < 0$. According to [1, 29] in the spin-isospin channel this curve can be considered as describing the π^+-type excitations. Another curve shown in Fig. 3 corresponds to the π^--type excitations. Their frequencies are to be taken with the opposite sign in respect to the ones shown in Fig. 3. There are two solutions for π^0-type excitations. One of them corresponds to the growing excitations (at $G' < -1$) and the second should be taken with the opposite sign and becomes to degenerate with the first one in the symmetric and asymmetric matter.

It is well known that the kinetic theory of Landau gives the linear dependence of frequencies of collective excitations on the wave vectors, i.e., $\omega \sim k$. When we pass to RPA using Eqs. (10), (12), the shape of the dependence changes and we obtain the branches of solutions $\omega_i(k)$. In Fig. 4 we show the imaginary branches $\omega_{sd}(k)$ obtained in RPA. The shaded fields on the edges of figures indicate that the branches are located on the unphysical imaginary axis. We see that the branches change continuously with G'. When $-1 < G' < 0$, the branches $\omega_{sd}(k)$ are located on the unphysical sheet only, but for $G' < -1$ they go over to the physical sheet in the interval of wave vectors $k = (0, k_{fin})$.

In analogy with Fig. 3, we can find the second solution of Eq. (1) for each values of G'

and k. The "symmetric" branch has the conjugated values on the physical sheet $\omega_{sd}^*(k)$, but it goes to the unphysical sheet $\tilde{I}$ when $k > k_{fin}$.

All solutions belong to the same family ω_{sd}. This family exists at $G' < 0$.

3.2 Pion dispersion equation

We consider the influence of the pion-nucleon interaction on the branches $\omega_{sd}(k)$. Following [1] we include only the direct term of the interaction of the pion with a particle-hole pair, and do not take into account the noncentral interaction of the quasiparticles. In this Section we take into account the isobar-hole pairs contribution to the pion self-energy, Eq. (8).

First let us investigate how the contribution of isobar-hole excitations changes the stability conditions. Let us assume in Eq. (19) that $\omega=0$ and $k \to 0$. In this limit this equation reduces to $-1 = \frac{1}{G'_{NN}}$. This gives the value of G'_{NN} when instability occurs in the long wavelength limit. If we take into account the isobar-hole loops, this condition takes the form

$$-4C_0\Phi_N(\omega = 0, k) \approx \frac{1 + C_0\frac{16}{9}\Phi_\Delta(0, k)G'^2_{\Delta\Delta}}{G'_{NN}(1 + C_0\frac{16}{9}\Phi_\Delta(0, k)G'_{\Delta\Delta}) - C_0\frac{16}{9}\Phi_\Delta(0, k)G'^2_{N\Delta}}. \tag{25}$$

At $\omega=0$ and $k \to 0$, $\Phi_\Delta(0, k)$ is proportional to nuclear density: $\Phi_\Delta(0, k) \approx \frac{\rho}{2(m_\Delta - m)}$. If $\rho \to 0$, the corrections produced by Φ_Δ disappear. As a result the values of ρ_c and k_c on the solid lines in Fig. 1 approach the dashed ones. In Fig. 1 the solid lines are obtained for the minimal densities when solutions with $\omega=0$ emerge for every G'_{NN}.

It is shown in Fig. 5a, how $\omega_{sd}^\pi(k)$ are modified when $f_{\pi NN}$ is changed from 0 to 1. At $f_{\pi NN}=0$ the branch of solutions of the zero-sound dispersion equation, Eq. (8), $\omega_{sd}(k)$ is presented. (It should be noted that the results in Fig. 5a are obtained for $\Pi_\Delta(\omega, k)$ contribution being included in pion self-energy (3) while those in Fig. 4 do not include $\Pi_\Delta(\omega, k)$.) As we see from Fig. 5a, the growth of $f_{\pi NN}$ results in emerging of the amplified solutions on the physical sheet at $-1 < G'_{NN} < G'_{tr}$.

In Fig. 5b the branches $\omega_{sd}^\pi(k)$ are shown for different values of density of nuclear matter. The curve 3 is calculated for $\rho = \rho_c$ and contains the point $\omega_{sd}^\pi(k_c)=0$. It is demonstrated how the zero value $\omega=0$ is placed on this branch (the point A). At the point A the condition $\left(\frac{d\omega_{sd}^\pi(k)}{dk}\right)_{k=k_c}=0$ is satisfied. The density ρ_c and wave vector k_c, corresponding to zero solution, are presented in Fig. 1 (denoted by A). When density is lower than the critical one, $\omega_{sd}^\pi(k)$ are completely situated on the unphysical sheet (curve 4) and the nuclear matter is stable. When $\rho > \rho_c$, the amplified solutions appear on the physical sheet in the certain interval of k (the curves 1 and 2).

Figures 5a, b demonstrate the typical behavior of the branches of solutions of (1) at $G'_{NN} < G'_{tr}$. Thus, we obtain the instability of nuclear matter related to $\omega_{sd}^\pi(k)$ for all $G'_{NN} < G'_{tr}$. Instability occurs at $\rho \geq \rho_c$. The corresponded solutions of the zero-sound dispersion equation, $\omega_{sd}(k)$, demonstrate instability at $G'_{NN} < -1$ only.

We refer $\omega_{sd}^\pi(k)$ to ω_{sd} family.

4 Investigation of instability at $G'_{NN} > G'_{tr}$

Now let us consider in Fig. 1 another well studied region $G'_{NN} \approx 2$. This region of G'_{NN} was investigated in connection with prediction of the pion condensation.

In Fig. 6 the solutions of Eq. (1) are presented at $G'_{NN} = 2$ and $\frac{\rho}{\rho_0}=1.78$. Such figures were published in papers [1]. In Fig. 6 we see the pion branch of solutions $\omega_\pi(k)$, it starts at the frequency $\frac{\omega_\pi(k=0)}{m_\pi} = 1$. It turns into the free pion solution as $f_{\pi NN} \to 0$. The isobar branch $\omega_\Delta(k)$ starts at the frequency which is determined by the isobar and nucleon mass difference. The zero-sound branch $\omega_s^\pi(k)$ starts at $\omega_s(k = 0)=0$, and at certain value of k it acquires an imaginary part due to Landau damping [22]. It goes over to unphysical sheet related to the cut II, Eq. (14), [2, 3]. Besides the numerated branches, one more imaginary branch is presented in Fig. 6. Let us denote it $\omega_c(k)$. Tracing of this branch of solutions stimulated development of the theory of the "pion condensation" [1].

In this Section we investigate the family of solutions ω_c and show that this family is responsible for the instability at $G'_{NN} > G'_{tr}$. In Fig. 6 a part of a branch $\omega_c(k)$ is presented that is located on the physical sheet in the interval $k_1 \leq k \leq k_2$. The rest of this branch is on the unphysical sheet I.

In Fig. 7 we present the same branch $\omega_c(k)$ as in Fig. 6, but here we show it from another point of view, i.e., considering the complex plane of ω (the solid line). The branch $\omega_c(k)$ starts at $k=0$ at the point '1' and has the real value $\frac{\omega_c(k=0)}{m_\pi} = 1$. With the increasing of k it moves to the unphysical sheet I. It follows from (18) that there is another branch of solutions $\omega'_c(k)$, which starts at the point $\frac{\omega'_c(k=0)}{m_\pi} = -1$ and is placed on the unphysical sheet I' (the dashed curve).

Below in paper, the hatching on the edge of figures with the right slope means that the drawing branches are located on the unphysical sheet I. The left slope means that they are on the sheet I'. The physical sheet is above the axis of abscissas.

In point '2' $\omega_c(k)$ and $\omega'_c(k)$ coalesce on the imaginary axis. Then $\omega_c(k)$ ascends the imaginary axis and $\omega'_c(k)$ descends. (To determine which of branches go up we can take into account the width of isobar in Eq. (5) as in [2].) Thus, two simple roots of Eq. (1) which move on the unphysical sheets I and I' (when k increase) coalesce on the imaginary axis at $k = k_m$. Here the roots become imaginary ones, and continue to move up and down the imaginary axis which belongs to both I and I' sheets.

In Fig. 7 the values of $\omega_c(k)$ and $\omega'_c(k)$ are shifted from the imaginary axis by hand to demonstrate the trajectories of solutions with increasing of k (it is shown by arrows). The wave vector $k = k_t$ corresponds to the turning point of the trajectories '3'. At this point, $\omega_c(k)$ and $\omega'_c(k)$ reach their maximal and minimal values. When $k > k_t$, the branches return along the imaginary axis. In Fig. 7 the solutions are presented for $k \leq 2.45 m_\pi$. At larger k, the behavior of branches has a nontrivial character but it is not related to physical processes and is not discussed here. In Figs. 6, 7 it is shown how 1) the branch $\omega_c(k)$ goes from the unphysical to the physical sheet at $k = k_1$; 2) it becomes imaginary, with growing value of $Im(\omega_c(k)) > 0$, on the physical sheet; 3) the branch returns to the unphysical sheet at $k = k_2$.

In Fig. 8 the complex plane of ω is presented where $\omega_c(k)$ and $\omega'_c(k)$ are shown for different densities of nuclear matter. In these figures (except Fig. 8a), the branches are drawn up to

the turning point on the imaginary axis, i.e., at $k = (0, k_t)$ (see Fig. 7). In Fig. 8a the density is small and the branches do not attain the imaginary axis. In Fig. 8b the branches encounter on the imaginary axis but completely stay on the unphysical sheets ($k_t = 1.78m_\pi$). In Fig. 8c the result for the critical density ρ_c is presented. On the real axis the solution with $\omega = 0$ appears. Here $k_t = k_c$ ($k_t = 1.81m_\pi$) and we see that the conditions $\omega_c(k_c) = 0$ and $\left(\frac{d\omega_c(k)}{dk} \right)_{k=k_c} = 0$ are satisfied. The wave vector and density corresponding to the point B in Fig. 8c are marked by B in Fig. 1. In Fig. 8d it is demonstrated that at $\rho > \rho_c$ the solutions with $Im(\omega_c(k)) > 0$ ($k_t = 1.88m_\pi$) exist on the physical sheet.

The critical densities and wave vectors in Fig. 1 for $G'_{NN} > G'_{tr}$ correspond to the solutions denoted by B in Fig. 8c. Such solutions $\omega_c(k)$ can be found not only when $G'_{NN} > G'_{tr}$, but for $G'_{NN} < G'_{tr}$ also. It should be mentioned, that an attempt to shift the pion condensation to larger densities means that $\omega_c(k)$ go on to stay on the unphysical sheet at larger densities. There are several reasons that can influence our results. It was shown in [2] that the important factor shifting the pion condensation to the larger densities is the decreasing of the effective nucleon mass with growth of density. This decreasing is predicted by the scaling of Brown-Rho [30] and QCD sum rules [31, 32]. However, at smaller values of the nucleon mass the lowest order expansion in powers of $\frac{p^2}{2m}$ in Eq. (9) is not valid any more, thus requiring relativistic kinematics for the nucleon. Besides, the formation of isobar Fermi surface must be taken into account, as soon as the density becomes so large that the quasiparticle energy on the Fermi surface exceeds the difference of the isobar and nucleon mass.

In Figs. 7, 8 the branches $\omega_c(k)$ start at the point $\omega_c(k=0) = m_\pi$. Inclusion of the scalar part of the pion self-energy Π_S, Eq. (2), displaces the initial value to $\omega_c^2(k=0) = m_\pi^2 + \Pi_S$ (Appendix A). However, this does not modify the curves in Fig. 1 qualitatively.

5 Determination of G'_{tr}

In Sects. 3, 4 we have presented zero-frequency solutions of Eq. (1), which appeared for different values of G'. In this Section the "transitional" value G'_{tr} is obtained. In Sects. 3,4 it was shown that at $G'_{NN} < G'_{tr}$ the zero-frequency solutions belong to the family ω_{sd} and at $G'_{NN} > G'_{tr}$ they refer to ω_c. In this Section the transition of solution with $\omega = 0$ from one family to another is demonstrated.

In the vicinity of G'_{tr}, at $G'_{NN} \approx G'_{tr}$, the branches belonging to ω_{sd}^π and ω_c families are placed close to each other on the same unphysical sheets. In Figs. 5, 7, 8 these branches are shown separately. In Fig. 9 the branches of the both families are shown simultaneously.

In Fig. 9a at $G'_{NN} = -0.0020$ and $\rho = \rho_c$, the branches $\omega_c(k)$, $\omega_c'(k)$ and $\omega_{sd}^\pi(k)$ are presented simultaneously. The critical value of the wave vector is $k_c = 1.61m_\pi$. The branches $\omega_c(k)$ and $\omega_c'(k)$ behave like in Fig. 8a. The branch $\omega_{sd}^\pi(k)$ is shown by the dotted curve and it is presented in the interval $k = (0, k_c)$. The behavior of $\omega_{sd}^\pi(k)$ is similar to the curve 3 in Fig. 5b between $k=0$ and the point A, which corresponds to $k = k_c$.

In Fig. 9a number '1' denotes the start of branches at $k=0$; '2' means the turning point of $\omega_{sd}^\pi(k)$: $k_t=0.077m_\pi$; '3' corresponds to $k=0.1m_\pi$. We see that $\omega_{sd}^\pi(k)$ descends when k changes from '0' to k_t and then ascends and turns to zero at $k = k_c$: $\omega_{sd}^\pi(k = k_c)=0$ (point C in Fig. 1).

Now let us enlarge a little the coupling constant: G'_{NN}=-0.0018. The following calculations are made at the critical density $\rho = \rho_c$, corresponding to this value of G'_{NN}. In this case we have a coalescence of $\omega_c(k)$ and $\omega'_c(k)$ on the imaginary axis. The wave vector of coalescence is equal to k_m=0.0962m_π. In this difficult for drawing case, the presentation of the branches is made in two steps. In Fig. 9b the branches are shown at $k \leq 0.094m_\pi$, i.e., before coalescence and in Fig. 9c at $k \geq 0.094m_\pi$. The position of branches at k=0.094m_π are marked by '2'.

In Fig. 9b it is shown that the position of $\omega^\pi_{sd}(k)$ at point '2' is much lower on the negative imaginary axis than the $Im\omega_c(k)$ and $Im\omega'_c(k)$. Further, in Fig. 9c we see the coalescence of $\omega_c(k)$ and $\omega'_c(k)$ at $k = k_m$ (point '3'). Then $\omega_c(k)$ and $\omega'_c(k)$ go in the opposite directions along the imaginary axis.

In Fig. 9c it is shown that the branch $\omega'_c(k)$ descends and meets the branch $\omega^\pi_{sd}(k)$ in the point '4' (at $\tilde{k}_m$=0.109m_π). [The branch $\omega^\pi_{sd}(k)$ has turned upward at k=0.104m_π.] After the second coalescence, the branches $\omega'_c(k)$ and $\omega^\pi_{sd}(k)$ go in the opposite sides on the complex plane. Thus, the branch $\omega'_c(k)$ has blocked $\omega^\pi_{sd}(k)$ on the unphysical sheet.

The branch $\omega_c(k)$ goes over to the real axis and a solution with ω=0 (point D) belongs to this branch: $\omega_c(k_c)$=0 at k_c=1.60m_π (the point D in Fig. 1).

Thus, the value of G'_{tr} is determined by the interaction of branches on the unphysical sheets shown in Fig. 9. We can conclude that G'_{tr} is a special value of the spin-isospin effective quasiparticle interaction when 1) there is coalescence of $\omega_c(k)$ and $\omega'_c(k)$ on the imaginary axis at the critical density $\rho = \rho_c$ and 2) $Im\omega^\pi_{sd}(k_m) \leq Im\omega_c(k_m), Im\omega'_c(k_m)$. The second condition is satisfied as a rule, since $Im\omega^\pi_{sd}(k_m)$ tends to $-\infty$ as $G' \rightarrow -0$ (compare with Fig. 3).

In Fig. 9 the results are presented for $\Pi(\omega, k) = \Pi_N(\omega, k)$ (2), i.e., without the excitation of isobars. In this case we have obtained G'_{tr}=-0.0019. If to solve Eq. (1) with $\Pi_P(\omega, k) = \Pi_N(\omega, k) + \Pi_\Delta(\omega, k)$, then G'_{tr}=0.0020. The influence of S-wave pion-nucleon interaction is discussed in Appendix A.

It is interesting to mention that the figure similar to Fig. 9 is presented in [20] for the solutions of the zero-sound dispersion equation. Their figure demonstrates the behavior of solutions for the different values of F_0 and the branches of solutions depend on F_1 instead of k (this means the dependence on the value of the quasiparticle effective mass m^* along the branch). In paper [20] F_0 and F_1 are the zero and the first multipolar components of the scalar-isoscalar effective interaction of the quasiparticles.

6   Discussion

A. In this paper two families of solutions to the pion dispersion equation are calculated, which determine the stability boundary of the nuclear matter (the critical density ρ_c) depending on the value of spin-isospin coupling constant G'. It is shown that there is a special value of $G' = G'_{tr}$ such that for $G' < G'_{tr}$ the stability boundary are related to the family ω^π_{sd} and for $G' > G'_{tr}$ it refers to ω_c.

It is interesting to investigate, whether we can obtain the information about the difference of the phase transitions at $G' < G'_{tr}$ and $G' > G'_{tr}$ using the branches of solutions. To do this let us consider the rate of growth of excitations in the vicinity of G'_{tr}. For $\rho > \rho_c$,

Eq. (1) has solutions with $Im\omega_i(k) > 0$. In Figs. 5, 7, 8d such solutions are presented. We determine $\Gamma(k) = -i\omega_i(k)$, $i = sd, c$. We can take several values of G' close to G'_{tr} and calculate the maximal values of $\Gamma(k)$ (i.e., $\Gamma(k_t)$) depending on ρ for the every G'. In Fig. 10 these results are demonstrated for $G' = G'_{tr}, G'_{tr} \pm 0.02, G'_{tr} \pm 0.2$, where G'_{tr}=-0.0019. In this figure we cannot observe the essential difference in the dependence of $\Gamma(k_t)$ on ρ for $G' < G'_{tr}$ and $G' > G'_{tr}$. It is possible to conclude that either this test is not sensitive to the type of excitations, or the character of the phase transition changes continuously with G' from long wavelength instability up to the pion condensation.

B. Now let us consider the singularity of the integrals containing the pion propagator D (1): $F = \int D(\omega, k) f(\omega, k) d\omega d^3k$, in the poles of $D(\omega, k)$ when $\rho = \rho_c$ and $k \to k_c$. The function $f(\omega, k)$ is not related to the poles of $D(\omega, k)$. In the Sect. 3.1 for the zero-sound dispersion equation (8), it was shown that there are two solutions on the physical sheet. At $-1 < G' < 0$, the amplified solutions go over to the unphysical sheets I, I' and the second branch goes over to the unphysical sheets $\tilde{I}$, $\tilde{I}'$ (Fig. 3).

Similar situation takes place for the pion dispersion equation. Up to now we considered the solutions which are located on the physical and unphysical I and I' sheets, but there are the "symmetrical" solutions. They have the conjugated values on the physical sheet and their unphysical sheets are $\tilde{I}$ and $\tilde{I}'$. This means that at $\rho = \rho_c$ and $k = k_c$ not only $\omega_i(k_c)$=0 ($i = sd, c$) but the "symmetrical" branch as well. As a result, the function F has a form (we leave the singular part only)

$$F \approx \int \frac{d\omega d^3k}{(\omega^2 - \omega_i^2(k))^2} f(\omega = 0, k_c).$$

Since we are interested in such zero solutions that $\left(\frac{d\omega_i(k)}{dk}\right)_{k=k_c}$=0, then $\omega_i = a(k - k_c)^2$ as $k \to k_c$ and the integral diverges along the curves in Fig. 1. This correspond to situation of the phase transitions [22].

C. In the paper we do not consider the case when $G'_{N\Delta}$, $G'_{\Delta\Delta}$ are modified simultaneously with G'_{NN}. But as it is shown above, the existence of G'_{tr} and $\omega_c(k)$, $\omega_{sd}(k)$ does not depend on whether we take excitation of the isobar into account or not. Therefore we do not expect the qualitative changes in our results if we change the values of $G'_{N\Delta}$ and $G'_{\Delta\Delta}$ together with G'_{NN}.

7 Conclusion

In the paper we investigate of the zero-frequency solutions of the pion dispersion equation depending on the values of the spin-isospin coupling constant of quasiparticles G'. For every G', the critical density ρ_c and the wave vector k_c corresponding to the solution with ω=0 were calculated. Then the branches of solutions, containing these zero solutions, are constructed and it is determined to what type of excitations (to what family) these solutions referred.

It is shown that the zero-frequency solutions belong to the different types of excitations, depending the value of G'. In all models used in calculations, the "transitional" value G'_{tr} ($|G'_{tr}| \ll 1$) is found, such that at $G' = G'_{tr}$ the zero solution passes from the branches of the type ω_{sd} to the ones of type ω_c.

At $G' < G'_{tr}$, the unstable amplified branches of solutions for the zero-sound dispersion

equation $(\omega_{sd}(k))$ and for the pion dispersion equation $(\omega_{sd}^\pi(k))$ are constructed (Figs. 3, 4, 5). In Fig. 5a we see that if to take the pion-nucleon coupling constant $f_{\pi NN}$ value to be very small, $\omega_{sd}(k)$ and $\omega_{sd}^\pi(k)$ are very close. When we increase $f_{\pi NN}$ up to 1, the behavior of $\omega_{sd}^\pi(k)$ is change: the damping solutions become amplified ones (Fig. 5). We obtain that the zero-frequency solutions of Eq. (1) at $G' < G'_{tr}$ belong to the same family of solutions which is responsible for the long wavelength instability in the kinetic theory of Landau.

Figure 1 demonstrates that the stability boundary continuously extends to $G' > G'_{tr}$. But at these G' the unstable solutions belong to family ω_c. It is shown that this family contents the solutions responsible for the pion condensation.

It is possible to expect that a new state of medium after phase transition is different depending the value of G'. We investigated the dependence of the maximal growth rate of perturbations at several G' in the vicinity of G'_{tr} on density. But this dependence does not exhibit the noticeable modifications at G'_{tr}.

8 Appendix A.

In this appendix the scalar part of the pion self-energy, Π_S, (2) and its influence on the behavior of the curves in Fig. 1 are considered. We construct Π_S using the relation of Gell-Mann–Oakes–Renner [2], [33]. It permits to express the pion mass in medium through the quark condensates in nuclear matter

$$m_\pi^{*2} = -\frac{\langle NM|\bar{q}q|NM\rangle(m_u + m_d)}{2f_\pi^{*2}} , \qquad (A1)$$

where m_u, m_d - masses of u- and d-quarks ($m_u + m_d$=11 MeV), f_π^* - coupling constant of the pion decay in the medium (here we assume that $f_\pi^* = f_\pi$=92 MeV, i.e., the vacuum and medium values of f_π coincide). The value $\kappa = \langle NM|\bar{q}q|NM\rangle$ is a scalar quark condensate in nuclear matter. It may be present as

$$\kappa = \kappa_0 + \rho\langle N|\bar{q}q|N\rangle + ... \qquad (A2)$$

Here κ_0 is a scalar quark condensate in vacuum, κ_0=-0.03 GeV^3; $\langle N|\bar{q}q|N\rangle$ is the matrix element of the scalar quark condensate calculated over the nucleon $\langle N|\bar{q}q|N\rangle \simeq 8$. Then from (A1) we obtain

$$m_\pi^{*2} = m_\pi^2 - \rho\frac{\langle N|\bar{q}q|N\rangle(m_u + m_d)}{2f_\pi^2} . \qquad (A3)$$

On the other hand, we can define m_π^{*2} using Eq. (1) as

$$m_\pi^{*2} = m_\pi^2 + \Pi(\omega, k = 0) . \qquad (A4)$$

The form of Π_S can be obtained comparing (A2) and (A3) provided that $\Pi_P(\omega, k = 0) = 0$

$$\Pi_S = -\rho\frac{\langle N|\bar{q}q|N\rangle(m_u + m_d)}{2f_\pi^2} . \qquad (A5)$$

In Fig. 1 the dotted lines correspond to the critical density ρ_c and wave vector k_c obtained for Eq. (1) with the pion self-energy (2). (Recall that for each G' in Fig. 1 we show the minimal ρ_c when solution $\omega=0$ appears). In this model the transition value of G' is $G'_{tr}=0.0026$.

9   Appendix B

Here we construct the unphysical sheets $\tilde{I}$ and $\tilde{I}'$. The solutions of Eq. (19) that are presented by the curve ab in Fig. 2 are placed on these sheets.

To pass on to the sheet $\tilde{I}$ we do the analytical continuation in ω of $ln(z) \equiv ln\left(\frac{\omega m}{\omega m - k p_F + \frac{1}{2}k^2}\right)$ from the lower edge of the cut I upwards, adding $2\pi i$ to $ln(z)$. The sheet $\tilde{I}$ is situated above the physical sheet. The value of $ln\left(\frac{\omega m}{\omega m - k p_F + \frac{1}{2}k^2}\right)$ above the upper edge of the cut I is $ln(-z) - \pi i + 2\pi i$. This expression is continued on the sheet $\tilde{I}$.

In similar way we construct the sheet $\tilde{I}'$ making the analytical continuation of $ln(z') \equiv ln\left(\frac{\omega m + k p_F - \frac{1}{2}k^2}{-\omega m}\right)$ from the lower edge of cut I', adding $2\pi i$ to logarithm values.

References

[1] A. B. Migdal, Rev. Mod. Phys. **50**, 107 (1978); A. B. Migdal, D. N. Voskresenskii, E. E. Saperstein, and M. A. Troitskii, Phys. Rep. **192**, 179 (1990).

[2] E. G. Drukarev, M. G. Ryskin, and V. A. Sadovnikova, Eur. Phys. J. **A4**, 171 (1999).

[3] V. A. Sadovnikova and M. G. Ryskin, Phys. At. Nucl. **64**, 440 (2001).

[4] R. F. Sawyer and D. J. Scalapino, Phys. Rev. **D7**, 953 (1973).

[5] G. E. Brown and W. Weise, Phys. Rep. **27**, 1 (1976).

[6] E. Oset, W. Weise, and H. Toki, Phys. Rep. **83**, 281 (1982).

[7] G. Mao, L. Neise, H. Stocker, and W. Greiner, Phys. Rev. **C59**, 1674 (1999).

[8] J. Helgesson and J. Randrap, Phys. Rev, **C52**, 427 (1995).

[9] C. Gale and J. Kapusta, Phys. Rev. **C35**, 2107 (1987).

[10] L. H. Xia, C.M. Ko, L. Xiong, and J. Q. Wu, Nucl. Phys. **A485**, 721 (1988).

[11] L. Liu and M. Nakano, Nucl. Phys. **A618**, 337 (1997).

[12] J. Diaz Alonso and A. Perez Canyellas, Nucl. Phys. **A526**, 623 (1991); L. Mornas, nucl-th/0107005.

[13] L. B. Leinson and A. Perez, Eur. Phys. J. **A20**, 371 (2004).

[14] M. F. M. Lutz, Phys. Lett. **B552**, 159 (2003); Phys.Lett. **B 566**, 277 (2003).

[15] S.-O. Backman, G. E. Brown, and J. A. Niskanen, Phys. Rep. **124**, 1 (1985).

[16] C. Garsia-Recio, E. Oset, and L. L. Salsedo, Phys. Rev. **C37**, 194 (1988).

[17] G. Chanfray and M. Ericson, Phys. Lett. **B141**, 163 (1984).

[18] J. Delorme and P. A. M. Guichon, Phys. Lett. **B263**, 157 (1991).

[19] M. Colonna and Ph. Chomaz, Phys. Rev. **C49**, 1908 (1994).

[20] C. J. Pethick and D. G. Ravenhall, Ann. Phys. **183**, 131 (1988).

[21] T. Ericson and W. Weise, *"Pions and nuclei"*, Clarendon Press, 1988.

[22] L. D. Landau and E. M. Lifshitz, *"Statistical physics"* (Pergamon Press, 1989).

[23] I. Ya. Pomeranchuk, Sov. Phys. JETP **8**, 361 (1958).

[24] D. Pines and P. Nozieres, *"The Theory of Quantum Liquids"* (W.A.Benjamin,Inc., 1966).

[25] H. Mueller and B.D. Serot , Phys. Rev. **C52**, 2072 (1995).

[26] J. Speth and E. Werner, W. Wild, Phys. Rep. **33**, 127 (1977).

[27] A. L. Fetter and J. D. Walecka, *"Quantum theory of many-particle systems"*(Mc-Graw-Hill, New York, 1971).

[28] W.H. Dickhoff, A. Faessler, J. Meyr-ter-Vehn, and H. Muthner, Phys. Rev. **C23**, 1154 (1981).

[29] S.-O. Backmann and W. Weise, *"Mesons in nuclei"*, v.III, 1095, Ed. by M. Rho, D. Wilkinson, (North-Holland Pub. Company, 1976).

[30] G. E. Brown and M. Rho, Phys. Rev. Lett. **66**, 2720 (1991).

[31] R. J. Furnstahl, D. K. Griegel, and T .D. Cohen, Phys. Rev. **C46**, 1507 (1992).

[32] E. G. Drukarev, M. G. Ryskin, V. A. Sadovnikova, Th. Gutsche, and A. Faessler, Phys. Rev. **C69**, 065210 (2004).

[33] M. Gell-Mann, R. Oakes, and B. Renner, Phys. Rev. **175**, 2195 (1968).

10 Figure captions

FIG. 1. Critical values of nuclear density ρ_c and wave vector k_c, at which in Eq. (1) solutions $\omega=0$ appear. Results for three models of the pion self-energy are presented: solid lines correspond $\Pi = \Pi_N + \Pi_\Delta = \Pi_P$ (2), (3); dashed curves are for $\Pi = \Pi_N$; dotted curves are for the total $\Pi = \Pi_P + \Pi_S$ (2).

FIG. 2. Complex plane of the frequency ω. a) Numbers I and II denote the cuts (14) of $\phi(\omega, k)$ and I' and II' denote the cuts of $\phi(-\omega, k)$; b) Unphysical sheets are shown: sheet I (the shading with the right slope) and sheet I' (the shading with the left slope).

FIG. 3. Solutions of Eqs. (22), (23), (24) at $G' < 0$ in the kinetic theory of Landau. The shading with the left slope marks unphysical sheet I and the horizontal shading refers to $\tilde{I}$. Results are obtained at $\rho = \rho_0$.

FIG. 4. Imaginary solutions $\omega_{sd}(k)$ to Eq. (19) obtained in RPA for following values of G': (1) -0.4; (2) -0.9; (3) -1.02; (4) -1.1; (5) -1.2. Results are obtained at $\rho = \rho_0$.

FIG. 5. Imaginary solutions $\omega_{sd}(k)$ of Eq. (8). a) Dependence of $\omega_{sd}(k)$ on $f_{\pi NN}$: the curve (1) $f_{\pi NN}=0$; (2) 0.4; (3) 0.6; (4) 1.0. The results are obtained at $\rho = \rho_0$ and $G'_{NN}=-0.4$. b) Dependence of $\omega_{sd}(k)$ on the value of density: the curve (1) $\rho/\rho_0=1$; (2) 0.318; (3) 0.265; (4) 0.221. The results are obtained at $f_{\pi NN}=1$ and $G'_{NN}=-0.4$. Point A marks solution with $\omega=0$.

FIG. 6. Different types of solutions of Eq. (1): spin-isospin zero-sound branch $\omega_s^\pi(k)$, pion branch $\omega_\pi(k)$, isobar branch $\omega_\Delta(k)$ and condensate branch $\omega_c(k)$. Results are obtained at $\frac{\rho}{\rho_0}=1.78$ and $G'_{NN}=2$. We computed that $k_1=1.35m_\pi$, $k_2=2.35m_\pi$.

FIG. 7. Branches $\omega_c(k)$ and $\omega'_c(k)$ on the complex plane of frequency. The shading with the right (left) slope marks the unphysical sheet I (I'). The physical sheet is above the abscissas axis. Axes of reference are shown by the dotted lines. The solid curve correspond to $\omega_c(k)$ and the dashed one is for $\omega'_c(k)$. The number '1' marks start of branches at $k=0$; '2' is the coalescence point at $k_m=1.28m_\pi$; '3' is the turning point at $k_t= 1.88m_\pi$. Variables $k_1, k_2, \frac{\rho}{\rho_0}$ and G'_{NN} are the same as in Fig. 6.

FIG. 8. Branches $\omega_c(k)$ and $\omega'_c(k)$ on the complex plane of frequency at different densities $\frac{\rho}{\rho_0}$. In figures b,c,d branches are shown at $k \leq k_t$. Point B marks solution with $\omega=0$. Notations of lines and sheets are the same as in Figs. 6, 7.

FIG. 9. Transition of a zero solution from family ω_{sd} to family ω_c. The solid, dashed and dotted curves denote $\omega_c(k)$, $\omega'_c(k)$ and $\omega_{sd}^\pi(k)$, correspondingly. a) $G'=-0.0020$. The number '1' corresponds to $k=0$; '2' means turning point of $\omega_{sd}^\pi(k)$: $k_t=0.077m_\pi$; '3' $k=0.1m_\pi$. Arrows show movement of branches with k. Point C corresponds to $\omega_{sd}^\pi(k_c)=0$. b) $G'=-0.0018$. Branches are shown for $k \leq 0.094m_\pi$ (point '2'). c) Continuation of figure b. Branches are shown for $k > 0.094m_\pi$. Point '3' marks the coalescence point of $\omega_c(k)$ and $\omega'_c(k)$ at $k=0.0962m_\pi$. Point '4' shows the coalescence point of $\omega'_c(k)$ and $\omega_{sd}^\pi(k)$ at $k=0.109m_\pi$. Point D corresponds to $\omega_c(k_c)=0$.

FIG. 10. Dependence of the maximal growth rate of fluctuations on density. The curve (1) corresponds to $G' = G'_{tr}=-0.0019$; (2) $G' = G'_{tr}-0.02$; (3) $G' = G'_{tr}+0.02$; (4) $G' = G'_{tr}-0.2$; (5) $G' = G'_{tr}+0.2$.
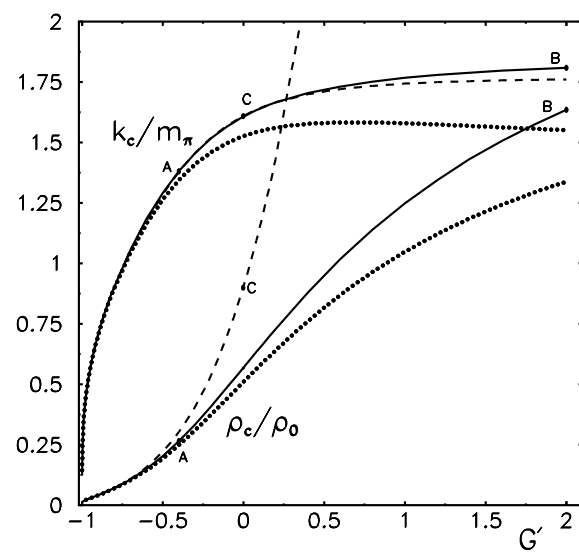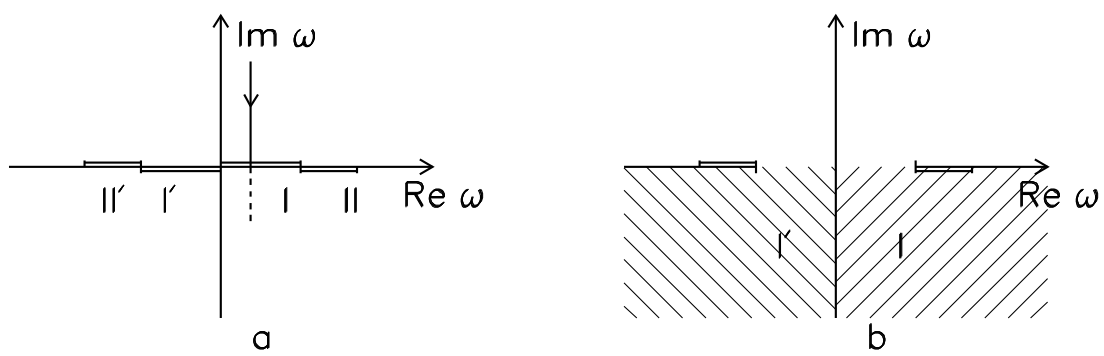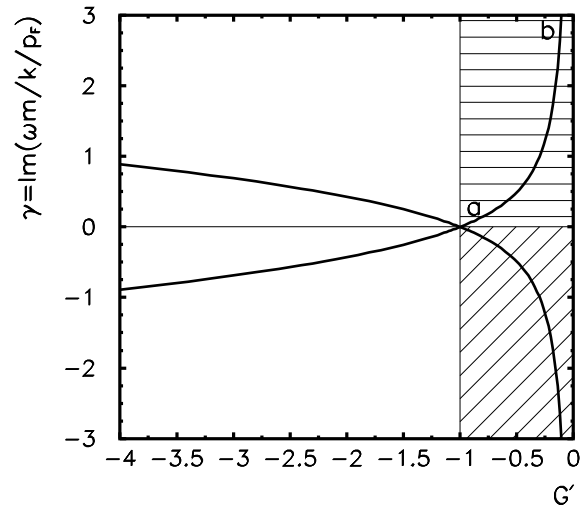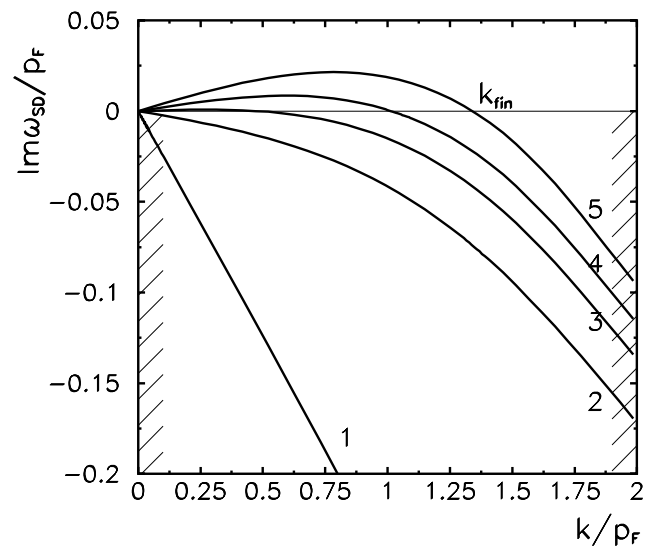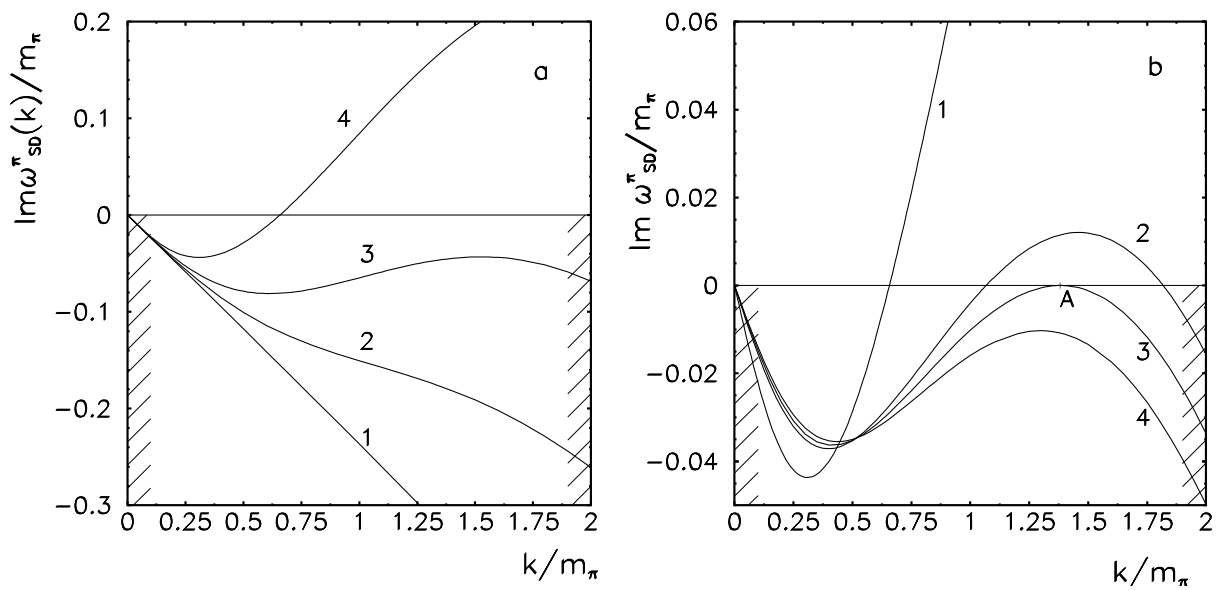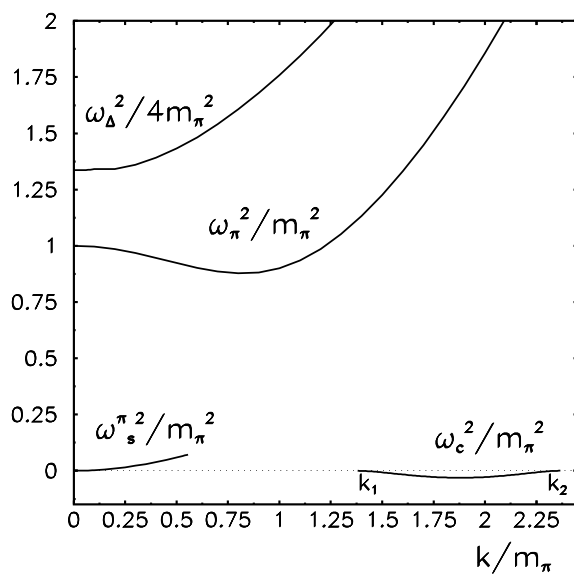
Figure 1:
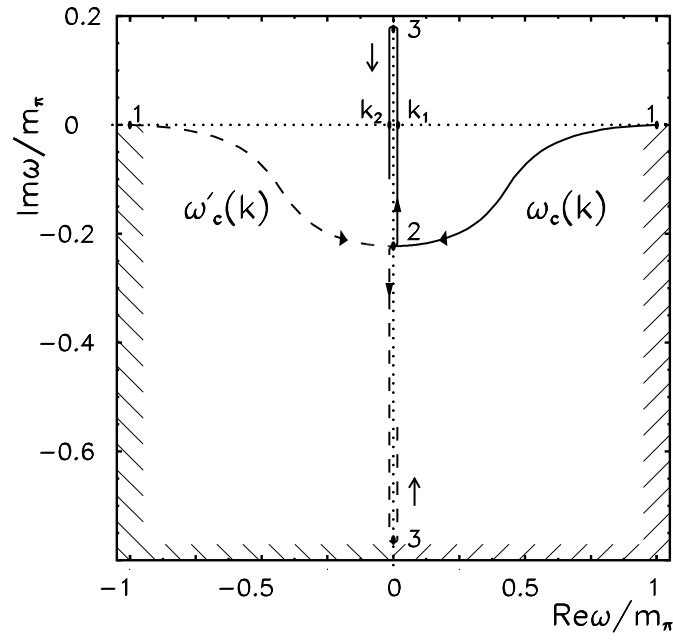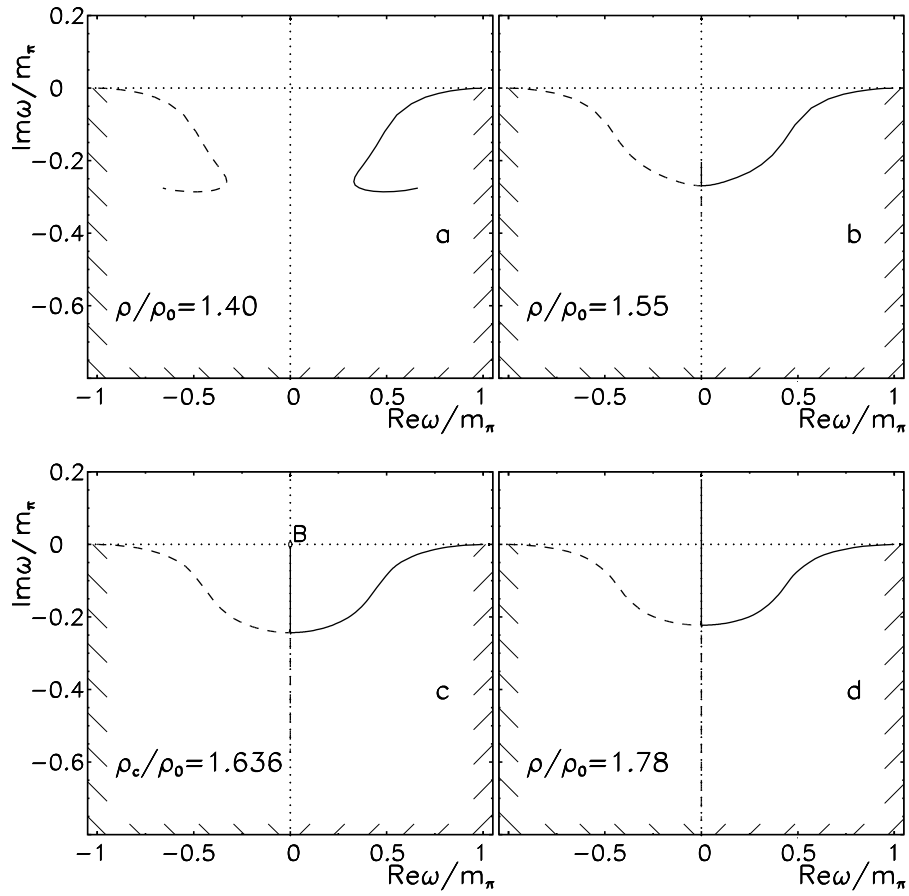

Figure 2:

Figure 3:

Figure 4:

Figure 5:

Figure 6:

Figure 7:

Figure 8:

Figure 9:

Figure 10: